Crystalline electric field effects in $PrNi_2B_2C$: Inelastic neutron scattering

Chandan Mazumdar,[1,2] M. Rotter,[3,*] M. Frontzek,[2] H. Michor,[4] M. Doerr,[2] A. Kreyssig,[2,5] M. Koza,[6] A. Hiess,[6] J. Voigt,[7] G. Behr,[8] L. C. Gupta,[9] M. Prager,[7] and M. Loewenhaupt[2]

[1]*Experimental Condensed Matter Physics Division, Saha Institute of Nuclear Physics, 1/AF Bidhannagar, Calcutta 700 064, India*

[2]*Institut für Festkörperphysik, Technische Universität Dresden, 01062 Dresden, Germany*

[3]*Institut für Physikalische Chemie, Universität Wien, Währingerstr. 42, 1090 Wien, Austria*

[4]*Institut für Festkörperphysik, Technische Universität Wien, 1040 Wien, Austria*

[5]*Ames Laboratory, Iowa State University, Ames, Iowa 50011, USA*

[6]*Institut Laue-Langevin, BP 156, 38042 Grenoble Cedex 9, France*

[7]*Jülich Centre for Neutron Science, Forschungszentrum Jülich, 52425 Jülich, Germany*

[8]*Institute for Solid State Research, IFW Dresden, D-01171 Dresden, Germany*

[9]*Max-Planck-Institut für Physik komplexer Systeme, D-01187 Dresden, Germany*

(Received 7 June 2008; published 28 October 2008)

$PrNi_2B_2C$ as a member of the borocarbide series is characterized by antiferromagnetic order below $T_N = 4$ K and the absence of superconductivity (at least down to 100 mK). There are two effects responsible for the absence of superconductivity in $PrNi_2B_2C$. These are the strong conduction electron–Pr moment interaction and a comparatively lower density of states. We studied the crystalline electric field (CEF) excitations and excitons in this compound by inelastic neutron scattering. The CEF level scheme obtained from these data comprises a singlet ground state, a doublet at 1 meV, and further higher levels at 5.2, 24.3 (doublet), 25.1, 29.4, and 31.5 meV. Large dispersion was found for the 1 meV excitation and explained theoretically taking into account magnetic exchange interactions. The calculated crystal-field parameters explain satisfactorily the neutron spectra as well as the heat-capacity and magnetic-susceptibility data. This leads to the conclusion that $PrNi_2B_2C$ can be described by the standard model of rare-earth magnetism. Thus the heavy-fermion concept, suggested by some groups earlier in literature, is not the cause of the suppression of superconductivity. Excitation spectra of the diluted series $Pr_{1-x}Y_xNi_2B_2C$ were also investigated. No drastic changes in the CEF level scheme have been observed in these compounds. Hence the CEF level scheme of the full compound, i.e., $PrNi_2B_2C$, is reasonably valid for these samples too. The superconducting-transition temperature $T_C \sim 15.5$ K for YNi_2B_2C decreases linearly with decreasing Y concentration x. Samples with $x \leq 0.65$ do not exhibit superconductivity down to 2 K.

DOI: 10.1103/PhysRevB.78.144422 PACS number(s): 71.70.Ch, 74.70.Dd, 75.10.Dg, 78.70.Nx

I. INTRODUCTION

RNi_2B_2C (R=Y, rare earth) compounds have been attracting attention right from the early days of their discovery.[1,2] They exhibit several unusual phenomena associated with the interplay of superconductivity and magnetism.[2,3] The magnetic-ordering and superconducting-transition temperatures observed for several compounds in this series are of the same order of magnitude.[3–5] The interplay of magnetic order and superconductivity has been studied extensively in $DyNi_2B_2C$ (T_C=6.0 K, T_N=10.6 K), $HoNi_2B_2C$ (T_C=8.0 K, T_N=8.5 K), $ErNi_2B_2C$ (T_C=11 K, T_N=6.8 K), and $TmNi_2B_2C$ (T_C=11 K, T_N=1.5 K) and their solid solutions.[5–8] On the other hand, $GdNi_2B_2C$ (T_N=19 K) and $TbNi_2B_2C$ (T_N=15 K) as well as the compounds containing light rare earths such as $PrNi_2B_2C$ (T_N=4.0 K) and $NdNi_2B_2C$ (T_N=4.8 K) are not superconducting but show magnetic order only.[6] $LuNi_2B_2C$ (T_C=16.5 K) and YNi_2B_2C (T_C=15.5 K) superconduct without exhibiting a magnetic order (no local or itinerant moment) down to low temperatures in the millikelvin range. Magnetic moments reside on rare-earth ions only and are strongly anisotropic due to the crystalline electric field (CEF) interaction.[6] Magnetic-ordering temperatures of the compounds given above follow the de Gennes scaling.[4] In some members of the series, magnetic properties are strongly influenced by $4f$ conduction-electron hybridization: $CeNi_2B_2C$ is a strongly mixed valence compound[2,3,9] and one report[10] claimed observation of a superconducting transition at ~100 mK [see Ref. 3 for discussion]. In $YbNi_2B_2C$, the $4f$ conduction-band hybridization is strong enough to suppress superconductivity, but is still not sufficient to affect Yb valence significantly. With Yb in a very closely 3+ state, $YbNi_2B_2C$ transforms into a heavy fermion at low temperatures, exhibiting a total loss of the Yb moment.[11,12] The rich spectrum of electronic and magnetic properties of RNi_2B_2C opened up a wide variety of investigations of several exotic phenomena.[3–5]

$PrNi_2B_2C$ undergoes an antiferromagnetic phase transition at T_N=4 K with a low ordered-moment of $0.8\mu_B$ pointing along the [110] direction,[6] much smaller than the free-ion value ($g_J J\mu_B = 3.2\mu_B$) and does not exhibit superconductivity down to 100 mK.[13] The relatively large value of T_N for $PrNi_2B_2C$ as compared to ~1 K expected from the de Gennes scaling in the series RNi_2B_2C (e.g., see Fig. 11 of Ref. 14) is a consequence of a large single-ion anisotropy and/or of $4f$(Pr) conduction-band hybridization. (See, e.g., the discussion on the archetypal high-T_N $PrBa_2Cu_3O_7$.[15]) Considering the small de Gennes factor of Pr, the absence of superconductivity in $PrNi_2B_2C$ can hardly be attributed to magnetic pair-breaking effects.[16] This led to speculation about anomalous heavy-fermion behavior of $PrNi_2B_2C$ by

Narozhnyi *et al.*[5] because valence fluctuations are known to suppress superconductivity as, e.g., observed in $La_{1-x}Ce_x$.[17] Alternatively, the absence of superconductivity in $PrNi_2B_2C$ may be due to unfavorable electronic band structure because in $LaNi_2B_2C$ superconductivity is also absent due to a markedly reduced electronic density of states at the Fermi level, $N(E_F)$, as compared to superconducting YNi_2B_2C and $LuNi_2B_2C$.[18,19] The fact that $N(E_F)$ of $PrNi_2B_2C$ is indeed rather close to the value for $LaNi_2B_2C$ has been demonstrated via a systematic band-structure study on RNi_2B_2C compounds.[20]

The aim of the present work is to investigate if magnetic properties of $PrNi_2B_2C$ can be accounted for by the standard model of rare-earth magnetism[21] with an appropriate CEF level scheme and if any evidence for anomalous heavy-fermion behavior and valence fluctuations can be found. Therefore, we have analyzed dc magnetic susceptibility,[22] specific heat, and the inelastic magnetic neutron response of Pr, both in $PrNi_2B_2C$ and in magnetically diluted $Pr_{1-x}Y_xNi_2B_2C$ compounds, where Pr^{3+} ions are more isolated from each other and pair correlations are weakened.

II. EXPERIMENTAL DETAILS

Polycrystalline samples of $Pr_{1-x}Y_xNi_2B_2C$ ($x=0,0.1,0.2,0.5,0.65,0.8,0.9,0.95,1$) were synthesized using the following procedure: appropriate amounts of Pr pieces, Ni powder, ^{11}B powder [which is necessary for inelastic neutron scattering (INS) because natural boron contains 19.4% ^{10}B, which strongly absorbs neutrons], and C powder were pelletized together and arc-melted under argon atmosphere. To ensure homogeneity, the resultant ingots were melted several times, turning them over after each melting. The total weight loss during the melting process was less than 1%. Finally, the compounds were melted in an induction furnace and cast in rods. These rods were wrapped in Ta foil, sealed in evacuated quartz tubes, and annealed at 1000 °C for 10 days and at 1100 °C for 1 day, and then quenched in cold water. Powder x-ray-diffraction (XRD) measurements, performed at room temperature using a Co Kα source, showed that the $Pr_{1-x}Y_xNi_2B_2C$ compounds are primarily single phase (space group, $I4/mmm$). No impurity peaks of appreciable intensity could be observed in the XRD data. The lattice parameters, as obtained from the analysis of the XRD data, are shown in Fig. 1. These values are in good agreement with those published in literature.[23] With increasing concentration x of yttrium, the lattice parameter a decreases following the usual lanthanide contraction, while c increases in accordance with the trend in RNi_2B_2C compounds.[3,4]

The superconducting properties were studied by ac-susceptibility measurements in the temperature range of 2–25 K using an Oxford Maglab susceptometer ($f=1000$ Hz). Heat-capacity measurements were carried out on samples of about 1.5 g in the temperature range of 1.5–150 K employing a quasiadiabatic step-heating technique.

Inelastic neutron spectra with incident energies of 25 and 56 meV were taken using the time-of-flight (TOF) spectrometer SV29 at the FZ Jülich to detect the crystal-field levels at higher energies. The powdered polycrystalline samples were placed inside flat aluminum boxes. The raw data were corrected for background and normalized to monitor. To study excitations at lower energies, TOF spectra were taken using the TOF spectrometer IN6 at ILL, Grenoble at temperatures between 2 and 200 K with an incident energy of 3.15 meV. With this setup the low-lying excited states ($\hbar\omega \leq 2$ meV) can be measured with better energy resolution at low temperatures in neutron energy loss, whereas the higher excited states are accessible by measuring the energy-gain spectra at higher temperatures. As was done in the experiment at the SV29 spectrometer, the sample was mounted using a flat aluminum box. The raw data were corrected for background and normalized with respect to a vanadium standard.

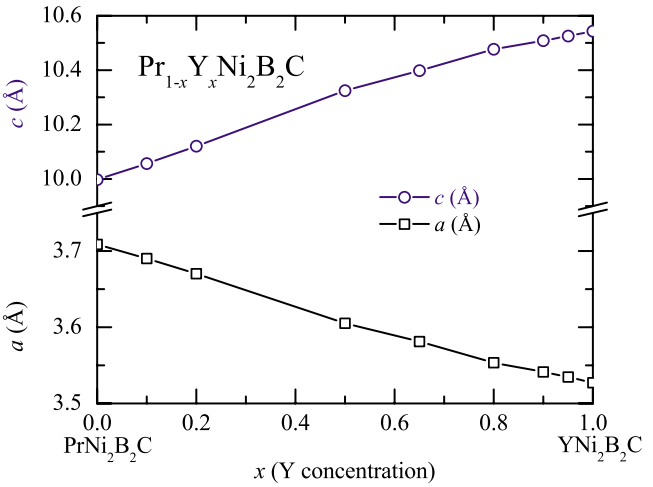

FIG. 1. (Color online) Variation in the lattice parameters of $Pr_{1-x}Y_xNi_2B_2C$. The lines are guides for the eyes.

III. RESULTS AND DISCUSSION

A. ac susceptibility

ac-susceptibility data at low temperatures are shown in Fig. 2. No superconductivity was observed for samples with $x \leq 0.65$, in agreement with results reported earlier.[23] Notice that the transition is sharp for the $x=1$ sample (containing no Pr ions), suggesting high quality of the pure sample YNi_2B_2C. In the samples that contain Pr ions, such as, for example, samples with $x=0.95$, 0.90, and 0.8, the superconducting diamagnetic response is somewhat broad due to compositional statistical fluctuations. dT_C/dx, the rate of change in T_C with respect to x, in the $Pr_{1-x}Y_xNi_2B_2C$ series is −35 K/mol Pr. This value is nearly the same as observed in doped $Gd_{1-y}Y_yNi_2B_2C$,[23,24] which suggests a similar influence on superconductivity of Pr and Gd ions introduced in dilute concentrations in YNi_2B_2C, though the origins of depression in T_C are completely different in the two cases. In the case of $PrNi_2B_2C$, it is due to band effects (see Sec. I) and in the case of $GdNi_2B_2C$ it is due to pair breaking. The magnetic ordering in $PrNi_2B_2C$ shows no signature in our ac-susceptibility measurements, in agreement with earlier reports that dc susceptibility in low external magnetic field (100 Oe) indicates only a deviation from Curie-Weiss behav-

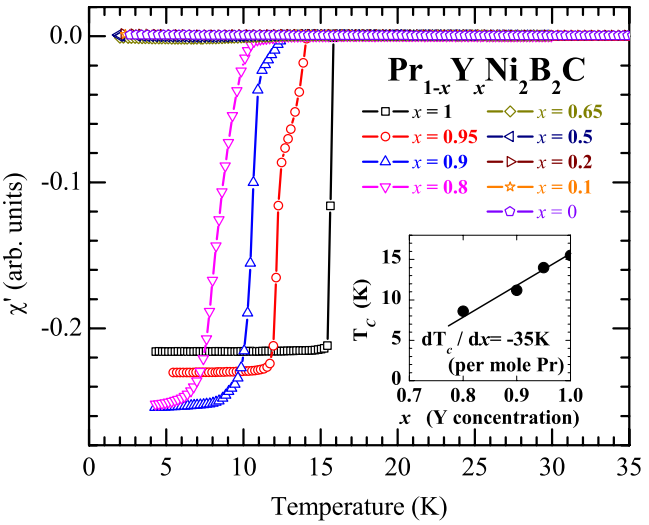

FIG. 2. (Color online) ac-susceptibility measurements on $Pr_{1-x}Y_xNi_2B_2C$. Samples with $x \leq 0.65$ do not show superconductivity down to 2 K. The inset shows T_C as a function of the concentration x.

ior below T_N=4 K.[25] As a signature of magnetic order, a broad maximum around T_N becomes better defined at a higher magnetic field (500 Oe). Our heat-capacity measurements, however, do show the magnetic transition clearly (see Fig. 9).

B. Inelastic neutron scattering

First we will present the inelastic-neutron-scattering spectra for the full compound $PrNi_2B_2C$ taken with different incident-neutron energies at temperatures between 2 and 150 K.[26] In Fig. 3, we show the spectra from counters with momentum transfers of less than 2 Å^{-1} where inelastic magnetic scattering is the dominant contribution to the scattering intensity. At the lowest temperature (2 K) the compound is in the magnetically ordered state. Therefore, the single-ion CEF transitions from the ground state to the excited states are modified due to the presence of two-ion exchange interaction. However, this modification is hardly visible for the high-energy transitions with energy transfers larger than 10 meV. It is masked by the considerably lower resolution of the SV29 data with incident energies of 56 meV. In this energy range (>10 meV) there is only one strong CEF transition at ~24.5 meV energy transfer that is visible. Because this transition is already observed at 2 K, it must connect the ground state with excited states lying around ~24.5 meV. For increasing temperatures its intensity is only slightly reduced, much less than expected from the inverse of the partition function. (See also Fig. 10: we expect a reduction to 70% at 10 K and to 40% at 50 K.) This indicates that for increasing temperatures there are additional transitions from a low-lying excited state (one doublet at 1 meV has indeed been determined as described later in the present study) to levels of ~25.1 meV.

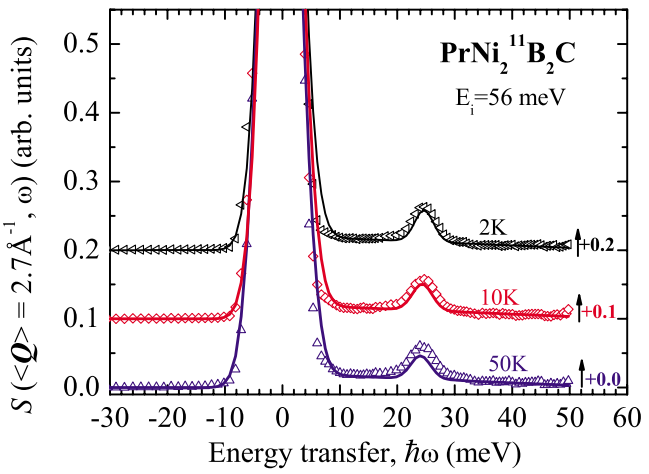

FIG. 3. (Color online) Inelastic-neutron-scattering spectra of $PrNi_2B_2C$ measured at SV29 with E_i=56 eV for different temperatures. Each spectrum has been shifted vertically for clarity. $\langle Q \rangle$ represents averaging for $Q=(2.70 \pm 0.49)$ Å^{-1}. The thick lines indicate the results of CEF calculations for 2, 10, and 50 K with an added elastic line (linewidth from vanadium measurement) and a straight-line background on the positive-energy-transfer side.

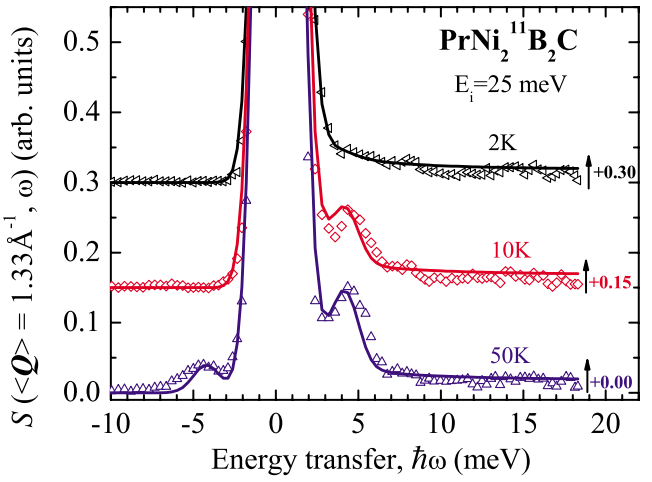

FIG. 4. (Color online) Inelastic-neutron-scattering spectra of $PrNi_2B_2C$ measured at SV29 with E_i=25 meV for different temperatures. Each spectrum has been shifted vertically for clarity. $\langle Q \rangle$ represents averaging for $Q=(1.73 \pm 0.31)$ Å^{-1}. The thick lines indicate the results of CEF calculations for 2, 10, and 50 K with an added elastic line (linewidth from vanadium measurement) and a small exponentially increasing background on the positive-energy-transfer side to model the intensity observed at T=2 K.

Magnetic excitations in the energy range of 3–15 meV are observed in the SV29 spectra taken with incident-neutron energy of 25 meV (Fig. 4). The dominant magnetic excitation at 4.5 meV is only seen at elevated temperatures; i.e., it must originate from an excited CEF level. Its temperature dependence suggests that this transition connects the CEF state at 1 meV with another excited state at (4.5+1) meV =5.5 meV. We also mention a rather weak excitation in the energy range around 8 meV which is already present at 2 K (hence it must originate from the ground state), but its temperature and Q dependence is unusual for CEF transitions. We, therefore, hesitate to assign a CEF level at 8 meV.

Up to now we have discussed the SV29 spectra considering only the neutron-energy-loss side (positive energy trans-

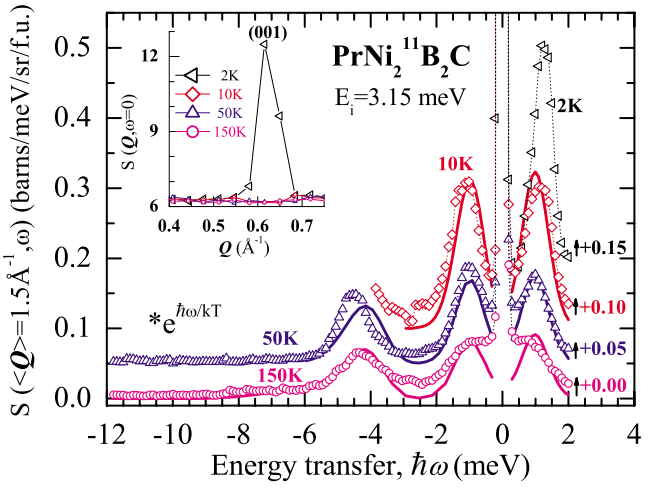

FIG. 5. (Color online) Inelastic-neutron-scattering spectra of $PrNi_2B_2C$ measured at IN6 with E_i=3.15 meV for different temperatures. The neutron-energy-gain spectra have been modified according to the detailed-balance condition. Each spectrum has been shifted vertically for clarity. $\langle Q \rangle$ represents averaging for Q =(1.5±0.1) Å^{-1}. The thick lines indicate the results of CEF calculations for 10, 50, and 150 K. The inset shows the presence of the magnetic (001) Bragg peak indicating the antiferromagnetic ordering at 2 K (T_N~4 K).

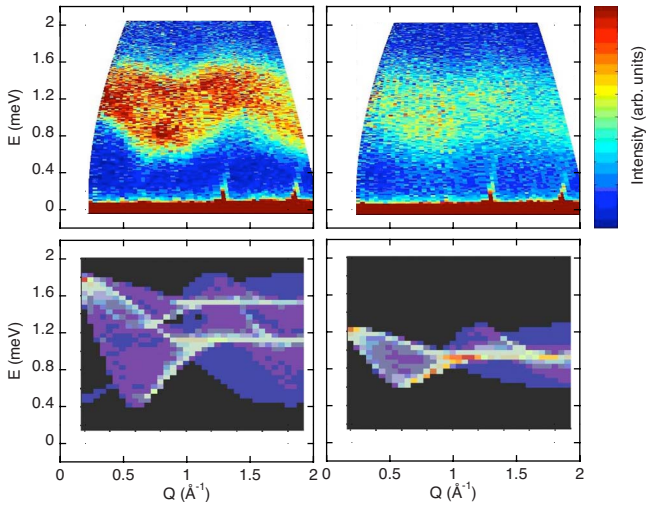

FIG. 6. (Color online) Inelastic-neutron-scattering spectra of $PrNi_2B_2C$ measured at IN6 at 2 K (top left) and 10 K (top right): a color-coded map of the neutron intensity vs energy and momentum transfer. For comparison, the figures at bottom left and bottom right show the results of the model calculation (for details see text).

fers). However, as can be seen in Fig. 4 in the spectrum at 50 K, there is also intensity at negative values of the energy transfer. In this part of the spectrum the neutron gains energy from the sample through the transition from a state at higher energy to a state at a lower energy. (Compare the 4.5 meV lines at both sides of the elastic line.) Intensities on both sides of the spectrum are related through the so-called detailed-balance condition, i.e., I(gain side) $=I$(loss side)$\exp[-\hbar|\omega|/k_BT]$. This fact has been used to present our IN6 data (Fig. 5) for both sides (neutron energy loss and gain). Multiplying the intensity on the gain side by $\exp[+\hbar|\omega|/k_BT]$, one obtains symmetric spectra and can compare the IN6 data on the energy-gain side directly with those of SV29 on the energy-loss side. Because of the much better energy resolution of IN6 [full width at half maximum (FWHM) at the elastic position is 0.1 meV for an incident energy of 3.15 meV], we can now also resolve the low-energy part (<2 meV) of the excitation spectrum in addition to the medium-energy range of up to 10 meV (the visibility of the latter, however, depending on temperature). A very strong CEF transition with energy of 1 meV is well resolved from the elastic line (which was not the case for the SV29 spectra). Plotting the intensity in the elastic window (±0.1 meV) as a function of the modulus of the momentum transfer $\boldsymbol{Q}$ (see inset of Fig. 5), one can also observe the (001) magnetic Bragg peak at 2 K indicating that the sample is in the magnetically ordered state and disordered for temperatures ≥10 K. The solid lines in the spectra in Figs. 3–5 correspond to a single-ion CEF model with parameters as given and discussed in Sec. III D.

In addition to the deduction of spectroscopic information from the low-temperature low-energy IN6 data, it is also possible to gain information on the dependence of the excitations on the modulus of the momentum transfer. (However, using a polycrystalline sample only the average over all three spatial directions is accessible.) This $\boldsymbol{Q}$-dependent information is especially important for the magnetically ordered state at 2 K. In addition to the single-ion CEF level scheme (which is by definition $\boldsymbol{Q}$ independent), we have to consider the two-ion exchange interactions, as stated in the beginning of this section. As we will see, the CEF ground state of the Pr^{3+} ion is a singlet and has no magnetic moment. Hence $PrNi_2B_2C$ should not order magnetically unless there is a strong CEF transition to a low-lying excited state that is able to induce a magnetic moment into the singlet ground state. In such a case a considerable dispersion will be observed—in other words, the CEF transition becomes an exciton.

Figure 6 (top left) shows the $\boldsymbol{Q}$-resolved magnetic excitations at 2 K in the energy range from 0 to 2 meV. At the elastic positions three magnetic Bragg peaks [(001) at 0.65 Å^{-1}, (100) at 1.70 Å^{-1}, and (003) at 1.88 Å^{-1}] and two nuclear Bragg peaks [(002) at 1.3 Å^{-1} and (101) at 1.81 Å^{-1}] fall into the accessible $\boldsymbol{Q}$ range. The observed band of excitations covers a range in energies between 0.4 meV (indicating a possible gap of this size) and 1.6 meV (upper boundary). Even in the paramagnetic state (Fig. 6, top right) we observe a band of excitations, though narrower and with less dispersion. A model calculation (see Sec. III D) assuming only nearest-neighbor exchange (that describes the magnetic structure correctly) is able to reproduce the main features of the observed excitations at 2 and 10 K as shown in Fig. 6 (bottom left and bottom right, respectively).

We now briefly discuss the influence of diluting the Pr^{3+} ions with nonmagnetic Y^{3+} ions. The inelastic-neutron-scattering energy spectra of $Pr_{0.9}Y_{0.1}Ni_2B_2C$, $Pr_{0.2}Y_{0.8}Ni_2B_2C$, and $Pr_{0.05}Y_{0.95}Ni_2B_2C$ were measured together with that of YNi_2B_2C as a reference which shows no appreciable intensities in the whole inelastic spectra. Figure 7 shows the spectra for $Pr_{0.9}Y_{0.1}Ni_2B_2C$ measured at different temperatures. As in the case of $PrNi_2B_2C$ (Fig. 5), the

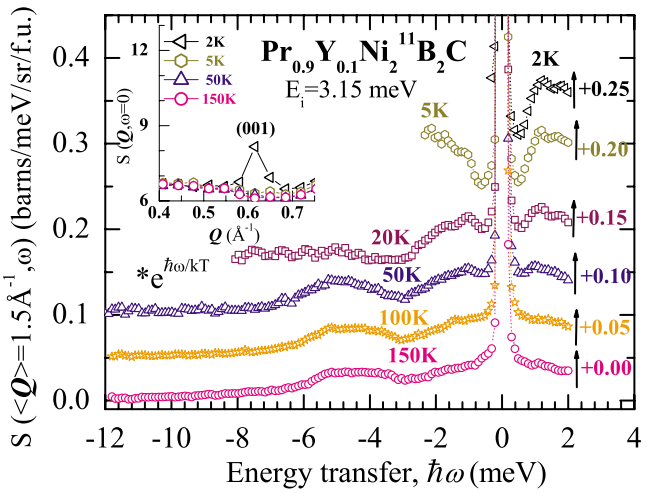

FIG. 7. (Color online) Inelastic-neutron-scattering spectra of $Pr_{0.9}Y_{0.1}Ni_2B_2C$ measured at IN6 with E_i=3.15 meV for different temperatures. The neutron-energy-gain spectra have been modified according to the detailed-balance condition. Each spectrum has been shifted vertically for clarity. $\langle Q\rangle$ represents averaging for $Q=(1.5\pm0.1)$ Å^{-1}. The inset shows the presence of the magnetic (001) Bragg peak indicating antiferromagnetic ordering at 2 K.

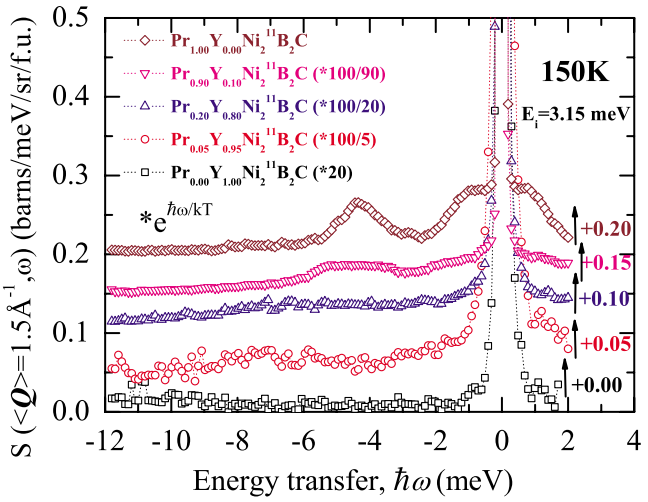

FIG. 8. (Color online) Inelastic-neutron-scattering spectra of $Pr_{1-x}Y_xNi_2B_2C$ for x=0, 0.1, 0.8, 0.95, and 1 measured at IN6 with E_i=3.15 meV at 150 K. The neutron-energy-gain spectra have been modified according to the detailed-balance condition. Each spectrum has been shifted vertically for clarity. $\langle Q\rangle$ represents averaging for $Q=(1.5\pm0.1)$ Å^{-1}. All spectra were scaled to Pr concentration, except that of YNi_2B_2C, where the scaling factor is the same (100/5=20) as that of $Pr_{0.05}Y_{0.95}Ni_2B_2C$.

spectra for $Pr_{0.9}Y_{0.1}Ni_2B_2C$ have also been scaled using the detailed balance factor ($e^{\hbar\omega}/k_BT$) in the neutron-energy-gain part. The features around 1 and 4.5 meV are still there but are much weaker and broader. The (001) magnetic Bragg reflection can also be observed (see inset of Fig. 7), but it is much weaker. The smaller intensity can be explained by a possible reduction in the magnetic-transition temperature in the diluted samples;[25] the moments are yet to attain saturation at 2 K. With Pr concentration decreasing further, the details of most of the features become less resolved and extremely weak; see Fig. 8.

C. Heat capacity

In order to obtain complementary thermodynamic information on the CEF scheme, we have analyzed the heat-capacity data shown in Fig. 9, which displays the magnetic contribution to heat capacity (ΔC_P vs T representation) in $PrNi_2B_2C$ in zero field. The phonon background has been estimated and subtracted using the heat-capacity data of $LaNi_2B_2C$.[25] The feature at $T\sim4$ K ($\sim T_N$) in $PrNi_2B_2C$ corroborates the magnetic phase transition to a long-range magnetic order.[6] The magnetic entropy was calculated from the magnetic specific-heat contribution, $S=\int(\Delta C_P/T)dT$, and is plotted in Fig. 9. As the lowest temperature for measurement of the heat-capacity data shown in Fig. 9 is 1.85 K, we added an estimate, $S(1.85\ \text{K})=0.35$ J/mol K. The entropy attains the value of R ln 3 at ~25 K, which indicates that the overall ground state is a quasitriplet, e.g., a singlet and a closely lying doublet.

As further analysis of heat-capacity data, we have calculated the single ion partition function z [$=\Sigma_j\exp(-E_j/k_BT)$] as a function of temperature applying the following formula:

$$F=\int SdT=-RT\ln z, \tag{1}$$

where F is Helmholtz free energy, and R is the molar gas constant. The results of this calculation are shown in Fig. 10. Within the CEF model, the single ion partition function is expressed as a sum over the different crystal field states j,

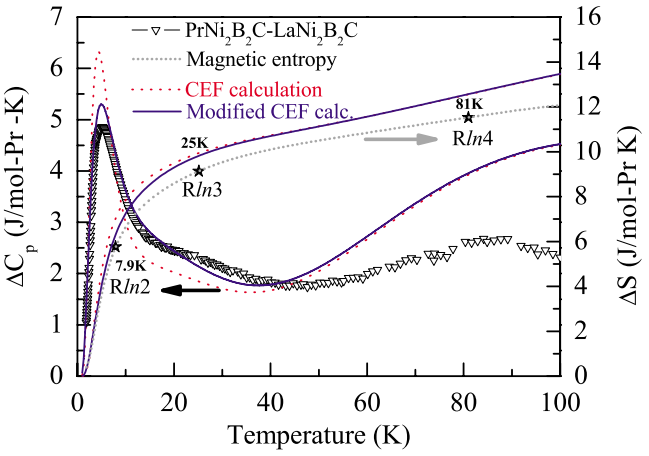

FIG. 9. (Color online) The magnetic contribution (4f) to heat capacity (ΔC_p vs T) in $PrNi_2B_2C$ deduced by subtracting the heat-capacity data of $LaNi_2B_2C$ (Ref. 25). Corresponding magnetic-entropy gain for $PrNi_2B_2C$ has been plotted in the same figure (right-hand-side axis). The dotted line represents the calculated magnetic heat capacity as derived from the CEF level scheme in the paramagnetic range. The thin solid line indicates the results of a model with a modified crystal-field level scheme in order to take into account qualitatively the effect of exchange interaction (see text).

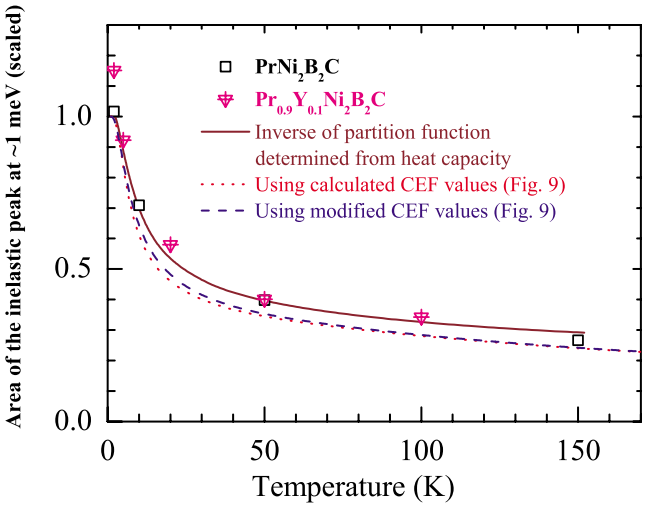

FIG. 10. (Color online) Temperature dependence of the (scaled) intensity of the inelastic peak at 1 meV in $PrNi_2B_2C$ and $Pr_{0.9}Y_{0.1}Ni_2B_2C$ measured at IN6 (see Figs. 5 and 7) and compared to the inverse of the partition function as deduced from heat-capacity data of $PrNi_2B_2C$ (solid line) and as calculated from the proposed CEF scheme (dotted line).

i.e., $z=\Sigma_j \exp(-E_j/k_BT)$ (here k_B denotes Boltzmann's constant). It is known that the temperature dependence of the intensity of CEF transitions that start from the ground state varies as $1/z$. We have calculated, at several temperatures, the integrated intensity of the inelastic neutron peak at ~1 meV for both $PrNi_2B_2C$ and $Pr_{0.9}Y_{0.1}Ni_2B_2C$. The results of these calculations are shown in Fig. 10. It is clearly seen that the intensities so calculated follow the variation in the inverse of the partition function with temperature. We have also calculated the partition function using CEF levels determined from the neutron data presented here, which also suggests the ground state as a singlet followed at 1 meV by a doublet or two very closely (~0.1 meV) lying singlets.

D. CEF calculations

The ground state of Pr^{3+} ions ($J=4$) has ninefold degeneracy. In the tetragonal point group D_{4h}, the multiplets split into five singlets ($\Gamma_{t1}^{(1)}$, $\Gamma_{t1}^{(2)}$, Γ_{t2}, Γ_{t3}, and Γ_{t4}) and two doublets ($\Gamma_{t5}^{(1)}$ and $\Gamma_{t5}^{(2)}$),[27] where the Γ_j are irreducible representations of the point group. It may be pertinent to note here that based on the extrapolation techniques (using a scaling factor)[28] from measurements on the rare-earth analog $TmNi_2B_2C$ (Tm^{3+}:$4f^{12}$), there are a couple of reports in literature on Pr CEF level schemes in $PrNi_2B_2C$.[29,30] However, the CEF line observed in our experimental data of $PrNi_2B_2C$ at ~1 meV does not appear in these extrapolated or calculated energy-level schemes of $PrNi_2B_2C$.[29,30] We may note here that often such calculations are in disagreement with the experimental results. For example, recently, Gasser *et al.*[30] demonstrated through polarized Raman-scattering studies in $ErNi_2B_2C$ that CEF levels extrapolated from low-energy inelastic-neutron-scattering data can be quite in disagreement with reality since analysis of the inelastic-neutron-scattering data for this system is quite difficult due to its crystal structure (a square-planar environment around the rare-earth ions). Although Divis *et al.*[31] also demonstrated that the calculated or extrapolated CEF level scheme for RNi_2B_2C can be in serious disagreement with the measured CEF values, their calculations also did not generate the CEF line at ~1 meV.

We have modeled the single-ion properties of $PrNi_2B_2C$ using CEF parameters that were derived using the MCPHASE package[32] by simultaneous fitting of dc-susceptibility data on single-crystalline compound,[33] as well as our inelastic-neutron-scattering and heat-capacity data on polycrystalline samples. The model Hamiltonian used is

$$\mathcal{H} = \sum_{ilm} B_l^m O_l^m(\vec{J}_i) - g_J \mu_B \vec{J} \cdot \vec{H}, \tag{2}$$

where the $4f$ moment of the ith Pr^{3+} ion is represented by the negative of the angular momentum operator[21] $\vec{J}_i$ and $\vec{J} = \Sigma_i \vec{J}_i$ is the negative of the total angular momentum operator. g_J is the Landé g factor and μ_B is the Bohr magneton. The first term in this expression is the CEF contribution and the second term is the Zeeman energy. The fit was restricted to the paramagnetic region only. In our initial attempt, we varied the parameter B_2^0 only in a narrow interval to have a correct description of magnetic susceptibility at high temperature. The magnetic-susceptibility behavior of single-crystalline tetragonal $PrNi_2B_2C$ is found to be very anisotropic in nature.[33] Therefore in the fitting procedure the statistical weights for different directions were chosen differently.

In a polycrystalline sample, neutron-diffraction cross section for a CEF transition $i \rightarrow i'$ (in units of b/sr meV) at a temperature T is expressed in dipole approximation as[34]

$$\frac{d^2\sigma(i \rightarrow i')}{d\Omega dE'} = \frac{k'}{k} S(Q,\omega) = N \frac{k'}{k} \left(\frac{\hbar \gamma e^2}{mc^2} \right)^2 e^{-2W} \left| \frac{1}{2} g_J F(Q) \right|^2 \frac{\exp(-E_i/k_BT)}{\sum_j \exp(-E_j/k_BT)} \times \sum_{\alpha=x,y,z} \frac{2}{3} |\langle i|J^\alpha|i'\rangle|^2 \delta(E_i - E_{i'} - \hbar\omega). \tag{3}$$

Here k'/k is the ratio of the momenta of the scattered and the incident neutrons, $4\pi(\hbar\gamma e^2/mc^2)^2$ is the total magnetic cross section (=3.65 b), $\gamma = g_n/2\hbar$ (g_n=1.913 042) is the gyromagnetic ratio of the neutron, and e^2/mc^2=2.82 fm is the classical electron radius. Furthermore, z [$=\Sigma_j \exp(-E_j/k_BT)$] is the single ion partition function, $\Sigma_{\alpha=x,y,z} |\langle i|J^\alpha|i'\rangle|^2$ is the sum of squares of the transition matrix elements of the angular momentum operator, and $\mathbf{F}(\boldsymbol{Q})$ is the magnetic form factor of the Pr^{3+} ion. In order to compare the cross section given in Eq. (3) to the experimental data, it was convoluted for each transition $i \rightarrow k$ by a Gaussian with an energy-dependent linewidth. As the spectra show a larger linewidth

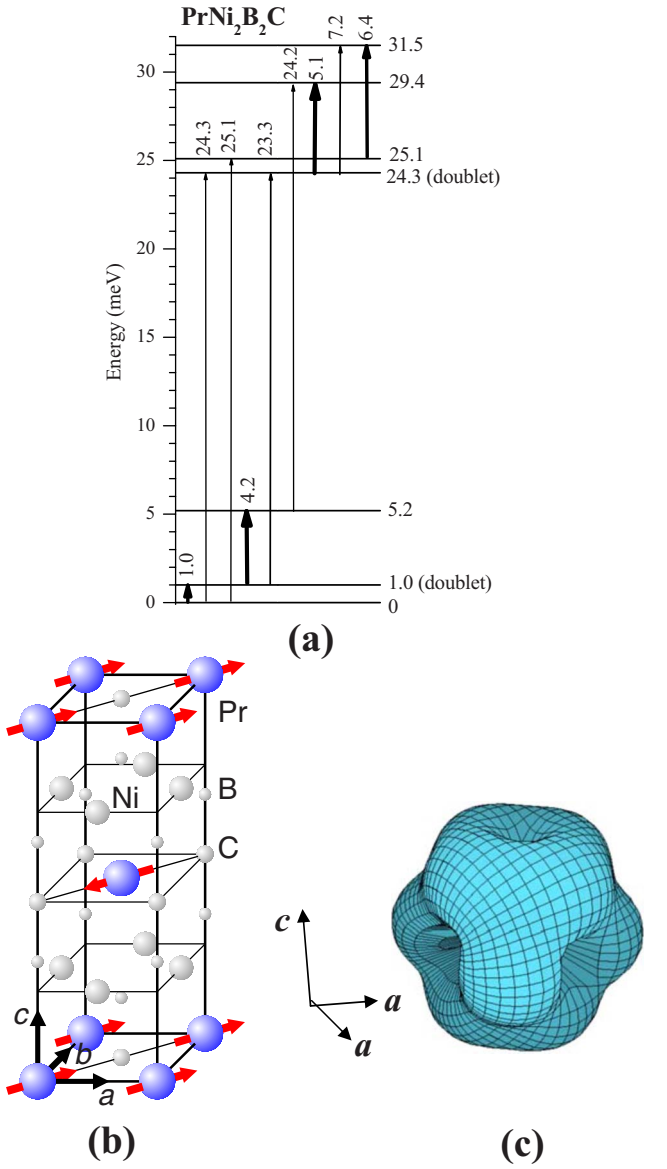

FIG. 11. (Color online) CEF splitting and charge density at $T=10$ K for Pr^{3+} in $PrNi_2B_2C$ as calculated from our CEF model (see text). For comparison the magnetic and crystal structure are shown.

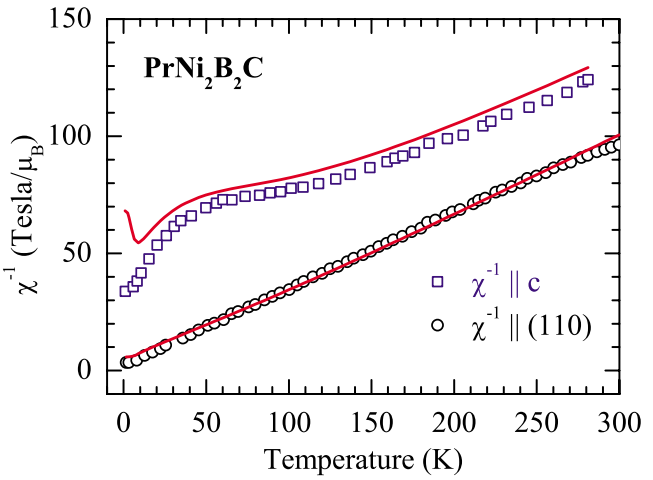

FIG. 12. (Color online) Inverse magnetic susceptibility of $PrNi_2B_2C$ along and perpendicular to the (110) plane (from Ref. 30). The solid lines represent susceptibility calculated from our proposed CEF model (see text).

than the experimental resolution of IN6, the linewidth was a parameter, which was fitted to the spectra.

Consideration of a singlet ground state and only a singlet at ~1 meV fails to explain all the experimental results simultaneously. In particular the calculated entropy would be much lower than the experimental one. The calculation yields the best fit for all three different experiments when the ground state is considered as singlet followed by a doublet at 1.0 meV, a singlet at 5.2 meV, another doublet at 24.3 meV, and singlets at 25.1, 29.4, and 31.5 meV, as shown in Fig. 11(a). The resultant crystal-field parameters obtained are $B_2^0=0.30$ meV, $B_4^0=3.0\times10^{-4}$ meV, $B_4^4=-7.4\times10^{-2}$ meV, $B_6^0=1.5\times10^{-4}$ meV, and $B_6^4=-4.9\times10^{-4}$ meV.

Our calculation suggests that the transition probability from the ground state to the level at 5.2 meV is zero. Neutrons can induce a transition to this excited state only from the doublet at 1.0 meV. The level scheme also explains the behavior of the magnetic entropy up to 50 K. At higher temperatures the experimental determination of the entropy is difficult and subtraction of the $LaNi_2B_2C$ probably overestimates the phonon contribution to the entropy. Considering the experimental errors the agreement of the fit to the heat-capacity (Fig. 9), neutron-intensity (Figs. 3–6), and magnetic-susceptibility (Fig. 12) data underlines that the crystal-field model shown in Fig. 11 is able to explain these physical properties.

In our analysis of the crystal-field results, we calculated the corresponding $4f$ charge density [see Fig. 11(c)]. There is a large variation in the tetragonal plane indicating an important influence of positive charges at the carbon neighbors in the tetragonal plane. On the other hand, the charge density is only slightly prolate in the $\boldsymbol{c}$ direction of the crystal. Such a distribution of charge density is associated with a planar anisotropy ([110] is the easy magnetic axis; see, e.g., Fig. 12). From the crystal-field anisotropy we expect that below T_N in the antiferromagnetic state the moments lie on the ab plane along the [110] direction, in agreement with the magnetic structure reported in literature.[6]

In order to interpret the $\boldsymbol{Q}$ dependence of the spectra, in particular in the magnetically ordered state at 2 K, the effect of exchange interactions has to be considered. This requires an extension of the simple crystal-field Hamiltonian [Eq. (2)] as

$$\mathcal{H}=\sum_{ilm}B_l^m O_l^m(\vec{J}_i)-g_J\mu_B\vec{J}\cdot\vec{H}-\frac{1}{2}\sum_{ij}J_{ij}\vec{J}_i\cdot\vec{J}_j, \qquad (4)$$

where J_{ij} is the exchange coupling between the angular momentum of the ith and jth Pr^{3+} ions. In a first simple model approach we introduced only one nearest-neighbor exchange interaction by setting $J(\frac{1}{2}\frac{1}{2}\frac{1}{2})=-15$ μeV. Using our crystal-field parameters in combination with a mean-field theory, this gives a magnetic-ordering temperature of $T_N=7$ K. This is a good estimate considering that in a mean-field model

critical fluctuations which suppress the order are neglected. In order to calculate the magnetic susceptibility below this temperature, assumptions about the distribution of the antiferromagnetic domains in the crystal have to be made. We assumed an ideal soft antiferromagnetic material. That is, by the application of a magnetic field along [110], only one domain showing the larger susceptibility was considered. This is the reason why the calculated susceptibility in the [110] direction does not show a maximum at T_N but continues to rise until saturation at temperatures well below T_N (see Fig. 12). On the other hand, for the susceptibility along [001] the calculation predicts a maximum, which is not found in the experimental data. However, considering the tiny signal in the hard direction, any misoriented small crystallite in the sample might contribute a large signal at low temperatures, which explains this discrepancy.

To calculate the effect of exchange interactions on the dispersion of the magnetic excitations, the random-phase approximation was adopted in a similar way as for $NdCu_2$.[35] In order to facilitate the computation of a polycrystalline average of the inelastic neutron cross section involving the calculation of spectra at many **q** vectors, a fast algorithm was used.[36] The result of such a powder average is shown in Fig. 6 (bottom left and bottom right) and can be compared with the experimental data taken at IN6 (Fig. 6, top left and top right). It can be seen that not only below T_N but also at higher temperatures the magnetic exchange interactions lead to some dispersion in the magnetic excitations.

In principle the interpretation of the specific-heat experiments should take into account this dispersive excitation spectrum. However, as there is no common consensus on how to implement this idea, we took into account the effect of dispersion by introducing an artificial splitting of the CEF doublet at 1.0 meV. The solid line in Fig. 9 shows the result of such a calculation [the CEF level scheme was set to 0, 0.8, 1.6, 5.2, 24.3 (doublet), 25.1, 29.4, and 31.5 meV], which clearly improves the theoretical description of the experimental specific-heat data.

IV. CONCLUSIONS

In conclusion, we report here detailed measurements on crystalline electric field levels in $PrNi_2B_2C$ and $Pr_{1-x}Y_xNi_2B_2C$. The CEF level scheme in $PrNi_2B_2C$ below 150 K consists of a singlet ground state, a closely spaced doublet at 1.0 meV, and a singlet at 5.2 meV. Also, our CEF calculations suggest a doublet at 24.3 meV and a singlet at 25.1 meV, the existence of which is indeed observed experimentally in time-of-flight neutron spectra. The correct CEF level scheme cannot be achieved by the extrapolation method using the spectra obtained in heavier rare-earth analogs. Our study demonstrates that in order to achieve reliable results, it is necessary to determine CEF model parameters by simultaneous fitting of many physical properties, i.e., heat capacity, magnetic susceptibility, and inelastic-neutron-scattering spectra. We find good agreement of the theoretical predictions of the CEF model with the experimental data in $PrNi_2B_2C$.

The excitations at 1.0 and 5.2 meV have also been observed in $Pr_{1-x}Y_xNi_2B_2C$ samples, but are much weaker and broadened. In view of the observed phase transition at high temperatures in DyB_2C_2 where quadrupolar ordering has been observed, the possibility of quadrupolar-induced magnetic transition in $PrNi_2B_2C$ must be considered and experimentally looked into. Recently, a similar phenomenon has been reported in $TmNi_2B_2C$.[37] The essential point of the present work is the determination of the CEF, which is of fundamental importance for the further investigation of the two-ion interactions (in particular their anisotropy), the coupling of magnetism to the lattice and to the conduction electrons in the system, which is important for the interplay of magnetism and superconductivity. For this purpose, neutron spectroscopic measurements on single crystals are required.

ACKNOWLEDGMENTS

This work was performed within the program of the Sonderforschungsbereich (SFB) 463 and supported financially by the Deutsche Forschungsgemeinschaft (DFG). The authors thank O. Stockert for providing software for the analysis of the IN6 data. M.R. and H.M. acknowledge support by the Austrian Science Foundation (FWF) under Projects No. P17226, No. P16957, No. P16250, and No. P16778. L.C.G. thanks MPIPKS for providing support and hospitality during his several visits. He also thanks Humboldt Foundation for the support during some of his visits to MPIPKS. The work by A.K. at Ames Laboratory was supported by the U.S. DOE under Contract No. DE-AC02-07CH11358. The authors are thankful to P. Fulde for his comments and suggestions that helped improving the paper.

*Present address: Clarendon Laboratory, Department of Physics, University of Oxford, Parks Road, Oxford OX1 3PU, UK.

[1] R. Nagarajan, C. Mazumdar, Z. Hossain, S. K. Dhar, K. V. Gopalakrishnan, L. C. Gupta, C. Godart, B. D. Padalia, and R. Vijayaraghavan, Phys. Rev. Lett. **72**, 274 (1994).

[2] R. J. Cava, H. Takagi, H. W. Zandbergen, J. J. Krajewski, W. F. Peck, Jr., T. Siegrist, B. Battlog, R. B. van Dover, R. J. Felder, K. Mizuhashi, J. O. Lee, H. Eisaki, and S. Uchida, Nature (London) **367**, 252 (1994).

[3] (a) See, for example, L. C. Gupta, Adv. Phys. **55**, 691 (2006); (b) R. Nagarajan, C. Mazumdar, Z. Hossain, and L. C. Gupta, in *Frontiers in Superconducting Materials*, edited by A. V. Narlikar (Springer-Verlag, Berlin, 2005), p. 393.

[4] K.-H. Müller and V. N. Narozhnyi, Rep. Prog. Phys. **64**, 943 (2001); K.-H. Müller, M. Schneider, G. Fuchs, and S.-L. Drechsler, in *Handbook on the Physics and Chemistry of Rare Earths*, edited by K. A. Gschneidner, Jr., J.-C. Bunzli, and V. K. Pecharsky (Elsevier, Amsterdam, 2007), Vol. 38, Chap. 239, pp. 175–336.

[5] V. N. Narozhyni, J. Freudenberger, G. Fuchs, K. A. Nenkov, D.

Eckert, A. Czopnik, and K.-H. Müller, J. Low Temp. Phys. **117**, 1599 (1999).
[6] J. W. Lynn, S. Skanthakumar, Q. Huang, S. K. Sinha, Z. Hossain, L. C. Gupta, R. Nagarajan, and C. Godart, Phys. Rev. B **55**, 6584 (1997).
[7] J. Freudenberger, A. Kreyssig, C. Ritter, K. Nenkov, S.-L. Drechsler, G. Fuchs, K.-H. Müller, M. Loewenhaupt, and L. Schultz, Physica C **315**, 91 (1999).
[8] A. Kreyssig, J. Freudenberger, C. Sierks, M. Loewenhaupt, K.-H. Müller, and N. Stuesser, Physica B (Amsterdam) **259-261**, 590 (1999).
[9] C. Mazumdar, E. Alleno, O. Sologub, P. Salamakha, H. Noel, M. Potel, A. D. Chinchure, R. Nagarajan, L. C. Gupta, and C. Godart, J. Alloys Compd. **339**, 18 (2002).
[10] M. El Massalami, R. E. Rapp, and G. J. Nieuwenhuys, Physica C **304**, 184 (1998).
[11] S. K. Dhar, R. Nagarajan, Z. Hossain, E. Tominez, C. Godart, L. C. Gupta, and R. Vijayaraghavan, Solid State Commun. **98**, 985 (1996).
[12] A. Yatskar, N. K. Budraa, W. P. Beyermann, P. C. Canfield, and S. L. Bud'ko, Phys. Rev. B **54**, R3772 (1996).
[13] M. El Massalami, H. A. Borges, H. Takeya, R. E. Rapp, and F. A. B. Chaves, J. Magn. Magn. Mater. **279**, 5 (2004).
[14] G. Hilscher and H. Michor, in *Studies of High Temperature Superconductors*, edited by A. V. Narlikar (Nova Science, New York, 1999), Vol. 28, p. 241.
[15] G. Hilscher, E. Holland-Moritz, T. Holubar, H.-D. Jostarndt, V. Nekvasil, G. Schaudy, U. Walter, and G. Fillion, Phys. Rev. B **49**, 535 (1994).
[16] P. Fulde, in *Handbook on the Physics and Chemistry of Rare Earths*, edited by Karl A. Gschneidner, Jr. and LeRoy Eyring (Elsevier, Amsterdam, 1979), Vol. 2, Chap. 17, pp. 295–386.
[17] B. Matthias, H. Suhl, and E. Corenzwit, Phys. Rev. Lett. **1**, 92 (1958).
[18] L. F. Mattheiss, T. Siegrist, and R. J. Cava, Solid State Commun. **91**, 587 (1994).
[19] H. Michor, T. Holubar, C. Dusek, and G. Hilscher, Phys. Rev. B **52**, 16165 (1995).
[20] M. Divis, K. Schwarz, P. Blaha, G. Hilscher, H. Michor, and S. Khmelevskyi, Phys. Rev. B **62**, 6774 (2000).
[21] J. Jensen and A. R. Mackintosh, *Rare Earth Magnetism: Structures and Excitations* (Clarendon, Oxford, 1991).
[22] H. Rho, M. V. Klein, and P. C. Canfield, Phys. Rev. B **69**, 144420 (2004).
[23] V. N. Narozhnyi, G. Fuchs, J. Freudenberger, K. Nenkov, and K.-H. Müller, Physica C **364-365**, 571 (2001).
[24] J. Freudenberger, G. Fuchs, K. Nenkov, S.-L. Drechsler, K.-H. Müller, and L. Schultz, Physica C **339**, 195 (2000).
[25] M. El-Hagary, Ph.D. thesis, Technische Universität Wien, 1999.
[26] A preliminary report on the initial measurements on $PrNi_2B_2C$ was presented by M. Rotter, C. Sierks, M. Loewenhaupt, J. Freudenberger, and H. Schober, in *Rare Earth Transition Metal Borocarbides (Nitrides): Superconducting, Magnetic and Normal State Properties*, NATO Advanced Study Institute, Series II: Mathematics, Physics, and Chemistry Vol. 14, edited by K.-H. Müller and V. N. Narozhyni (Kluwer, Dordrecht, 2001), pp. 137–154.
[27] A. M. Mulders, A. Yaouanc, P. Dalmas de Réotier, P. C. M. Gubbens, A. A. Moolenaar, B. Fåk, E. Ressouche, K. Prokes, A. A. Menovsky, and K. H. J. Buschow, Phys. Rev. B **56**, 8752 (1997).
[28] C. A. Morrison, *Angular Momentum Theory Applied to Interactions in Solids*, Lecture Notes in Chemistry Vol. 47, edited by G. Berthier *et al.* (Springer-Verlag, New York, 1988), p. 119.
[29] U. Gasser, P. Allenspach, F. Fauth, W. Henggeler, J. Mesot, A. Furrer, S. Rosenkranz, P. Vorderwisch, and M. Buchgeister, Z. Phys. B: Condens. Matter **101**, 345 (1996).
[30] U. Gasser, P. Allenspach, J. Mesot, and A. Furrer, Physica C **282-287**, 1327 (1997).
[31] M. Divis, J. Rusz, G. Hilscher, H. Michor, P. Blaha, and K. Schwarz, Czech. J. Phys. **52**, 283 (2002).
[32] http://www.McPhase.de/; M. Rotter, J. Magn. Magn. Mater. **272-276**, E481 (2004).
[33] V. N. Narozhnyi, G. Fuchs, J. Freudenberger, K. A. Nenkov, D. Eckert, A. Teresiak, A. Czopnik, and K.-H. Müller, in *Rare Earth Transition Metal Borocarbides (Nitrides): Superconducting, Magnetic and Normal State Properties*, NATO Advanced Study Institute, Series II: Mathematics, Physics, and Chemistry Vol. 14, edited by K.-H. Müller and V. Narozhnyi (Kluwer, Dordrecht, 2001), p. 181.
[34] P. Fulde and M. Loewenhaupt, in *Spin Waves and Magnetic Excitations*, edited by A. S. Borovik-Romanov and S. K. Sinha (Elsevier, Amsterdam, 1988), Chap. 6.
[35] M. Rotter, S. Kramp, M. Loewenhaupt, E. Gratz, W. Schmidt, N. M. Pyka, and B. Hennion, R. v. d. Kamp, Appl. Phys. A: Mater. Sci. Process. **74**, S751 (2002).
[36] M. Rotter, Comput. Mater. Sci. **38**, 400 (2006).
[37] N. H. Andersen, J. Jensen, T. B. S. Jensen, M. v. Zimmermann, R. Pinholt, A. B. Abrahamsen, K. Nørgaard Toft, P. Hedegård, and P. C. Canfield, Phys. Rev. B **73**, 020504(R) (2006).